Tuning the material and catalytic properties of SUZ-4 zeolites for the conversion of methanol or methane

Michael Dyballa[1,2,*], Dimitrios K. Pappas[1], Elisa Borfecchia[3,4], Pablo Beato[3,*], Unni Olsbye[1], Karl Petter Lillerud[1], Bjørnar Arstad[2], and Stian Svelle[1,*]

[1]*Center for Materials Science and Nanotechnology (SMN), Department of Chemistry, University of Oslo, 1033 Blindern, 0315 Oslo (Norway)*
[2]*SINTEF Materials and Chemistry, Forskningsveien 1, 0373 Oslo (Norway)*
[3]*Haldor Topsøe A/S, Nymøllevej 55, 2800 Kgs. Lyngby (Denmark)*
[4]*Department of Chemistry and INSTM Reference Center, University of Turin, via P.Giuria 7, 10125 Turin (Italy)*

** Corresponding author: Michael Dyballa, E-mail: m.m.dyballa@smn.uio.no; Pablo Beato, E-mail: PABB@topsoe.com; Stian Svelle, E-mail: stian.svelle@smn.uio.no;*

Abstract

This work describes the synthesis and investigation of improved SUZ-4 catalysts (SZR framework) and their application in methanol-to-olefins and methane-to-methanol conversion. We report boron containing, dealuminated and desilicated SUZ-4 catalysts. Ammonia and pyridine probe molecules enabled the assignment of acid site densities to the 10-MR and 8-MR pores, respectively. The difference in between the theoretically expected and the for the probes accessible acid site density is a good descriptor for the accessibility of pores and acid sites. The access to the 8-MR SUZ-4 pores is sterically hindered by counter ions as well as extra framework aluminum (EFAl) species that account for up to 15% of the aluminum. Dealumination and desilication were successfully applied to optimize the diffusion properties and resulted in outstandingly high BET surface area, n_{Si}/n_{Al}-ratios and potassium exchange degrees. The improved accessibility led to an up to 2-fold increased MTO conversion capacity of the catalysts. Cu-exchanged SUZ-4 was applied in the selective oxidation of methane to methanol. By *operando* X-Ray absorption spectroscopy (XAS) we showed that Cu^{II} ions are mainly coordinated in 2Al sites of 6-MR motifs and inhibited for redox-reactions.

Keywords

SUZ-4; methanol-to-olefin conversion (MTO); methane to methanol conversion; desilication; probe molecules

Highlights

Successful synthesis of new SUZ-4 catalysts, including boron-incorporation into SZR framework

Desilication and dealumination applied to SUZ-4 catalysts

Acid site location and accessibility determined by combination of standard methods

Investigation of counter ion nature and location giving new insights into methane oxidation

New SUZ-4 catalysts with remarkable properties

1. Introduction

Among heterogeneous catalysts, zeolites possess properties that make them outstandingly useful as catalyst with high selectivity. Their microporous silica framework possesses incorporated heteroatoms like aluminum that, with a proton counter ion, result for example in Brønsted acidity. The second main property is the shape-selectivity, resulting from the limited space that is accessible for molecules in pores of different shape and size [1]. These properties can be used to manipulate reactions in a desired way, for example in case of the methanol-to-olefins (MTO) conversion [2]. A summary focused on existing kinetic models and of the reaction conditions for the MTO process was given by Keil [3]. The intersecting 10- and 8-MR pores of the SUZ-4 topology bear not only potential as shape-selective catalysts in the MTO conversion but were after copper exchange also applied to activate C-H bonds during the in methane-to-methanol conversion [4, 5].

The 3-dimensional SZR pore system of SUZ-4 consists of a straight 10-membered ring (MR) pore (diameter 5.2 x 4.1 Å) and two intersecting 8-MR zigzag pores (diameter 4.8 x 3.2 Å and 4.8 x 3.0 Å) [6]. It is thereby closely related to the 2-dimensional FER pore system consisting of a straight 10-MR (diameter 5.4 x 4.2 Å) and a perpendicular intersecting, straight 8-MR (diameter 4.8 x 3.5 Å). However in the SUZ-4, although the pores are intersecting and form a 3-D framework, the mass transport is limited because the 8-MR zigzag pores are partially blocked by non-exchangeable potassium ions. As shown by Lawton et al. [7] the potassium is in addition also trapped inside 6-MR cages. Problematic for the accessibility of the pores are also extra-framework aluminum (EFAl) species that were reported to exist in SUZ-4 [8]. However, their quantity, nature, and their location remain unknown.

SUZ-4 zeolites are scarcely investigated or applied in reactions since Lawton et al. [7] published in 1993 the crystallographic details of the structure. They pointed out the regular locations of potassium counter ions and were able to exchange ~40% of all potassium present after the synthesis. Zholobenko et al. [9] investigated a SUZ-4 with n_{Si}/n_{Al}-ratio 6.2 by IR spectroscopy and NH_3-TPD. They related bridging OH-groups located in 10-, 8- and 6-MR structures giving rise to IR bands at 3610, 3592 and 3565 cm^{-1}, respectively. Their assignment of the first two bands were supported by NH_3 adsorption and desorption experiments and allowed the authors to estimate the amount of acid sites located in 10- and 8-MR channels to 50 and 40%. IR spectra further revealed that the acid sites in 10-MR and 8-MR show different accessibility for *i*-butane and *n*-hexane.

Teketel et al. [8] investigated the acidity of a SUZ-4 with n_{Si}/n_{Al}-ratio 8 by TPD and FT-IR, showing an accessibility of acid sites to n-propylamine of 0.63 mmol/g and to pyridine of 0.2 mmol/g. Due to diffusion limitations, not all acid sites were accessible to pyridine. This made the

quantification of Lewis acidity impossible. The needle-like crystals furthermore showed a surprisingly high selectivity to light olefins in the MTO conversion. This was explained by the large number of 8-MR pore openings perpendicular to the needle main axis, in contrast to few 10-MR openings. Gao et al. [10] investigated different gel compositions in the SUZ-4 synthesis. By replacing 2/3 of KOH by NaOH and applying a complex re-use of the seed slurry from previous syntheses, they managed to vary the framework n_{Si}/n_{Al}-ratios between 5.3 and 9. They did neither investigate specifically protic forms nor in particular the acid site density (ASD) of the SUZ-4 catalysts. In a following study they also synthesized long needles of SUZ-4 catalysts with n_{Si}/n_{Al}-ratio 5.3 and were able to resolve by FT-IR spectroscopy two different acid sites in 10-MR (3610 cm^{-1}) and 6-MR (3558 cm^{-1}), the latter being a rather broad shoulder [11]. Katada et al. [12] investigated a SUZ-4 catalyst with n_{Si}/n_{Al}-ratio 6.5 by ammonia IR-MS-TPD and quantified the acid site density of the 3610 cm^{-1} band to 0.36 mmol/g (16% of aluminum contributes to acid sites). Gujar et al. [13] characterized both protonic and copper-exchanged SUZ-4 catalysts of unpublished n_{Si}/n_{Al}-ratio using Raman spectroscopy. They assigned Raman bands to the SUZ-4 framework and template, but did not discuss the accessible acid sites quantitatively. Cu^{2+}-exchange of the catalysts and aging (4 h at 1073 K in water saturated gas stream of 21%O_2/Ar) resulted in less intense low-frequency Raman bands of copper-oxo species explained by a less homogeneous distribution of copper after aging. Summarizing, all until now published acid site densities (ASD) are far below the densities that could be expected from the n_{Si}/n_{Al}-ratio of the reported SUZ-4 catalysts (in previous studies always below 10). This indicates that a large fraction of the present aluminum does not lead to (accessible) acid sites.

It is the aim of this publication to investigate the impact of post-modifications on the accessibility of acid sites and on the catalytic performance of SUZ-4 catalysts. As post-modifications, alkaline and/or acid treatment is applied in different severity to remove deposits and to dealuminate the zeolite. Similar techniques have led to reduced ASD for the comparable zeolite Ferrierite [14, 15], and to significant improvements in the performance of unidimensional ZSM-22 catalysts [16, 17]. Another possibility to modify the ASD and strength is the incorporation of other heteroatoms than aluminum, for example of boron [18, 19]. We herein report for the first time the synthesis of boron containing SUZ-4 catalyst and give information on the influence of gel aging. The Brønsted and Lewis ASD of all catalysts were estimated by indirect methods (elemental composition, MAS NMR) and direct measurement conducted using probes of different kinetic diameter, namely ammonia (0.375 nm) and pyridine (0.533 nm) [20]. Furthermore, we investigate the use of the SZR topology in the methane-to-methanol conversion after a copper exchange. After a stepwise activation process, Cu_xO_y species reactive towards the selective oxidation of the methane are generated. In particular the 8-MR pore of SUZ-4 is expected to be able to host the active site [4].

2. Experimental

2.1. Syntheses and post-modifications

The parent SUZ-4 catalyst S0 was synthesized according to literature [8]. Briefly, 0.4 g elemental aluminum was diluted in a solution of 3.3 g KOH in 51 ml distilled water. When the solution was clear, 5.8 g tetraethylammoniumhydroxide solution (25%, Sigma-Aldrich) and 19 g Ludox AS-40 (Sigma-Aldrich) were added slowly and the solution stirred for 10 min in the elemental composition $7.9K_2O$: Al_2O_3 : $16.5SiO_2$: 1.83TEAOH : $500H_2O$. The synthesis was conducted hydrothermally in tumbling 30 ml stainless-steel autoclaves with Teflon inserts at 433 K for 5 days (no differences to 7 days observed). The synthesized zeolite was separated by centrifugation, washed three times with distilled water and calcined for 12 h at 823 K in flowing air. The resulting catalyst was two times exchanged using 10 wt% NH_4NO_3 solution and washed three times with distilled water. To get the H-form of the zeolite, ammonia was burned off at 773 K for 4 h. Further aging of the synthesis gel (more than 1 h prior to crystallization) leads to a dumbbell-like shaped catalyst. It is shown in Fig. S1 in the supporting information (SI). This catalyst was named S02 and is not part of the main article. Frequently after the aging a mixture of both shapes S0 and S02 is obtained.

The SUZ-4 catalyst with co-incorporated boron and aluminum, S0B, was synthesized using two separate solutions for the respective reagents. For the first solution, 0.5 g boric acid was diluted in a solution of 3.0 g KOH and 22 ml distilled water. Subsequently, 5.8 g tetraethylammoniumhydroxide solution (25%, Sigma-Aldrich) and afterwards 19 g Ludox AS-40 (Sigma-Aldrich) were added. A second solution of 0.28 g elemental aluminum and 3.0 g KOH diluted in 31 ml water was prepared. The first solution was slowly added to this second solution and the combined solution stirred for 20 min in the elemental composition $10.6K_2O$: Al_2O_3 : 0.81 B_2O_3 : $25SiO_2$: 3.2TEAOH : $760H_2O$. The synthesis was conducted hydrothermally in tumbling 30 ml stainless-steel autoclaves with Teflon inserts at 433 K for 5 days. Further treatments were applied as stated above.

To synthesize S1K, the parent zeolite S0 was treated at 348 K for 40 h using 15 ml/g 0.5 M K_2CO_3 solution and subsequently washed with water. The catalyst was exchanged with NH_4NO_3 and the ammonia burned off at 773 K for 4 h. The catalyst was then stirred twice at 333 K for 3 h using 50 ml/g 0.1 M HCl solution. To synthesize S1Na, the parent zeolite S0 was desilicated at 348 K for 1 h using 30 ml/g 1 M NaOH stirred solution and subsequently washed with water. The catalyst was stirred twice at 333 K for 3 h using 50 ml/g 0.1 M HCl solution. To synthesize S2N, the parent zeolite S0 was dealuminated under reflux at 353 K over 24 h using 50 ml/g in 68% (15 M) HNO_3 and subsequently washed until NO_3^--free. The copper-exchanged catalyst S3Cu was synthesized by

exchanging the parent H-SUZ-4 catalyst (S0) in a 0.1 M solution of copper(II)acetate (Sigma-Aldrich) at a pH between 5.5 - 6.0 for 16 h (pH adjusted with 28 wt% NH_4OH-solution and 0.1 M HNO_3). The catalyst was finally three times washed with distilled water to remove excess copper. Before measurements all catalysts were activated for 12 h at 773 K in air (heating rate 1 K/min).

2.2. Characterization

X-ray diffraction (XRD) patterns were obtained on a Bruker D8 Discovery diffractometer using Cu-Kα radiation (λ=1,5418 Å). Patterns were collected in a 2Θ range from 2 to 70° in Bragg-Brentano geometry. The relative crystallinity was determined as the ratio between crystal scattering and amorphous scattering using the Bruker software EVA. Crystallite size was determined using the column height method (LVol-IB) based on peak integral width from a Pawley fit in the Topas V5 software. N_2-physisorption measurements were conducted using a BELsorp mini II instrument at 77 K. Prior to the measurements, the samples were activated in vacuum at 80 °C for 1 h and at 300 °C for 2 h. The specific surface areas were calculated using the Brunauer-Emmett-Teller equation (BET) at relative pressure p/p_0 below 0.1. The mesoporous Volume V_{meso} was evaluated using the t-plot method and subtracting the total pore Volume V_0 (at p/p_0 = 0.99) by the micropore Volume V_m. Scanning electron microscopy (SEM) images were taken on a Hitachi SU8230 instrument. For the detection of nanoparticles, a high-angel backscattered electron detector (BSE) was used. The elemental composition, especially n_{Si}/n_{Al}-ratio, n_K/n_{Al}-ratio and n_{Cu}/n_{Al}-ratio, were determined by energy-disperse X-ray spectroscopy (EDX) at 20 kV accelerating voltage on 200 x 200 µm areas of pelletized catalyst. Quantification was performed using a Bruker Quantax system consisting of a X-flash 6|10 detector and Esprit software. The water content of the catalysts was determined using a Stanton Redcroft TGA instrument by heating the catalysts at 1 K/min to 573 K in dry synthetic air and maintaining that temperature for 1.5 h. The coke content was determined from the TGA weight loss after dehydration. The sample was heated at 1 K/min to 1073 K and that temperature maintained for 1.5 h.

^{1}H, ^{11}B, ^{27}Al, and ^{29}Si MAS NMR single pulse spectra were collected on a Bruker Avance AV III 500 MHz WB Spectrometer at SINTEF, Oslo (NO), using 3.2 mm and 4 mm (just for ^{29}Si) zirkonia rotors at a spinning frequency of 20 kHz or 8 kHz, respectively. Applied resonance frequencies were 500.13 MHz for protons, 160.46 MHz for boron, and 157.97 MHz for silicon. Aluminum was measured at 130.32 MHz using 10000 π/12 pulses. The spectra were referenced to TMS (^{1}H), 0.5 wt% $B(OH)_3$ solution (^{11}B), 1M $Al(NO_3)_3$ solution (^{27}Al), and TMS (^{29}Si) and processed using Bruker TopSpin software and Dmfit V32 [21]. Before ^{1}H MAS NMR measurements, the sample was dried in the 3.2

mm rotor under vacuum at 423 K, 573 K, and 723 K for 1.5 h for each step. Ammonia was introduced via a vacuum line at a pressure of 60 mbar over 10 min. Surplus ammonia was removed in vacuum for 10 min at RT followed by 2h at 473 K. The dry samples were opened and sealed in a glove box purged with dry argon.

FT-IR spectroscopy was performed on a Bruker Vertex 80 spectrometer on self-supporting wafers of catalyst that were placed in gold envelopes. Briefly, catalyst pellets were subsequently activated in vacuum for 1.5 h at 423 K, 573 K, and 723 K. They were loaded with pyridine via a vacuum line. Surplus pyridine was removed in vacuum at 473 K for 2h. Bands at 1547 cm^{-1} and 1455 cm^{-1} were quantified as Brønsted and Lewis acid site densities, respectively, applying previously determined correction factors and the mass density of the dry pellet.

Operando XAS measurements were conducted at the BM26 beamline of the European Synchrotron Radiation Facility (ESRF), using the microtomo reactor cell designed by the ESRF environmental group connected to a gas delivery setup [22]. The powdered catalyst was measured as self-supporting wafer of optimized thickness (ca. 110 mg of catalyst for 1.3 cm^2 area pellet resulting in an edge jump $\Delta\mu x \sim 0.5$ for a total absorption after the edge of $\mu x = 2.5$). The catalyst was heated to 773 K at a rate of 5 K/min in O_2 flow (15 ml/min) and activated for 2 h, then cooled down to 473 K in O_2 and subsequently flushed with He. CH_4 loading took place at the same temperature (473 K) methanol was desorbed by steam assisted extraction obtained by feeding a helium flow (25 ml/min) through a water-filled bubble saturator into the cell. Reaction products were followed by a Pfeiffer Omnistar mass spectrometer. *Operando* Cu K-edge XAS spectra were acquired in transmission mode, using a Si (111) monochromator for the incident energy scan and ionization chambers for the detection of incident (I_0) and transmitted (I_1) photons. All the collected XAS spectra were normalized to the unity edge jump using the Athena software from the Demeter package [23]. The extraction of the $\chi(k)$ function was also performed using the Athena program, and FT-EXAFS spectra were obtained by calculating the Fourier transform of the $k^2\chi(k)$ functions in the (2.4 – 12.0) $Å^{-1}$ k-range.

2.3. Catalytic testing

Catalytic testing of H- SUZ-4 catalysts in the methanol-to-olefin conversion was performed in an atmospheric pressure rig at 673 K at WHSV of 0.5 and 0.2 $g_{MeOH}g_{Cat}^{-1}h^{-1}$. The equivalent of 100 mg dry catalyst in sieve fraction 425 to 250 µm was loaded in a U-shaped quartz reactor (I.D. = 6 mm). Prior to reaction, the catalyst was activated in synthetic air for 8 h at 823 K. Methanol was introduced by a He-stream passing through a bubble saturator at 353 K. The methanol partial pressure was

controlled via a condenser kept at 293 K. The effluent was analyzed by an on-line Agilent 6890N gas chromatograph equipped with an Agilent HP-PLOT Q capillary column (15 m).

S3Cu was tested in the conversion of methane-to-methanol in a quartz plug flow reactor (I.D. = 6 mm). Typically, 100 mg in sieve fraction 425 to 250 µm were used for the stepwise conversion (3 Steps: a) high temperature activation in oxygen; b) methane loading; c) steam-assisted methanol extraction). First, the catalyst was dried in helium flow (15 ml/min) at 423 K; then an O_2 flow (15 ml/min) was introduced and the temperature was raised with 5 K/min to 773 K, where it was kept for 480 min. After activation, the temperature was decreased to 473 K with a rate of 5 K/min in O_2 flow. The system was purged with helium for 60 min and dry CH_4 was introduced at a flow of 15 ml/min over 360 minutes at 473 K. The catalyst was again purged with helium and finally a water saturated stream of neon/helium (15 ml/min at 318 K) was passed through the reactor. The effluent was analyzed by a Hewlett Packard 6890/5972 GC-MS. Further details can be found elsewhere [24].

3. Results

3.1. Physical properties gained by standard characterization techniques

X-ray diffraction (XRD) patterns of the zeolites can are shown in Fig. 1. All of them show the characteristic reflection peaks of the SZR topology. No reflection peaks of competing crystal structures or impurities appear. However, the most intense (110) reflection peak decreases due to different water contents inside the zeolite pores and a changing crystallite size. Moreover, the (001) reflection peak at 11.9° decreases remarkably after post-modifications. It is sharp compared to the Pawley fit (not shown) and the relative high-angle intensities are maintained. This reflects the needle-like crystal shape, being elongated along the z-axis in [001] direction (direction of the 10-MR pore).

Fig.1

The relative crystallinities of the catalysts and other characterization data is summarized in Tab. 1. The directly synthesized catalysts S0 and S0B have relative crystallinities of 90% and 95%, respectively, showing a high degree of order and less amorphous contributions in the boron containing sample. The relative crystallinities of the soft alkaline-treated material S1K (90 %), the acid dealuminated material S2N (90 %) and the copper-exchanged S3Cu (90 %) are within the error comparable to the parent material. A slightly lower relative crystallinity of 80% was observed after strong desilication (S1Na). Thus, the amount of amorphous material increases after dissolving parts of the catalyst. The obtained crystallite sizes are simulated on the basis of spherical particles though the catalyst crystals are of needle-shape. Resulting size values are thus averaged over the actual crystal size and shape distribution. These values are not of direct physical meaning but can be compared in between the different catalysts. This is necessary to get representative crystal sizes also taking into account hidden crystals in the SUZ-4 agglomerates. From the simulated sizes it becomes clear that all post-modifications decrease the average size of the crystals. This is in accordance with the changing low-angle reflection peak intensities in Fig. 1. On the other hand, directly synthesized S0B with a higher relative crystallinity tends to form bigger crystallites. The weighted-profile *R*-factor (R_{WP}) of the simulations was below 11 indicating a satisfactory accuracy of the results and crystallite sizes.

We will first focus on the attempts to obtain the directly synthesized materials. SEM images of SUZ-4 catalysts can be found in Fig. 2. The image of S0 shows the parent SUZ-4 as synthesized in the well-known, hedgehog-like agglomeration (Fig. 2, top panels). An identical shape and agglomeration is seen for catalyst S0B with boron in the framework. The agglomerates consist of needle-shape crystals with 10-MR pores running parallel to the crystal main axis as described in literature [8, 11]. According to N_2-physisorption, no significant difference in BET surface area or mesopore volume (V_{meso}) is observed for the boron containing catalyst S0B compared with S0 (see Tab. 1). The BET values of directly synthesized SUZ-4 S0 and S0B are close to 346 m^2/g reported for directly synthesized SUZ-4 catalysts previously [8]. Both directly synthesized catalysts S0 and S0B have a comparable water content of 8-9% at RT under atmospheric conditions. However, a quite different, dumbbell-like shape can be synthesized by aging the gel (see SI, Fig. S1). It is noteworthy that attempts to reduce the initial aluminum content of S0 by changing the synthesis gel composition (reduced aluminum content and alkalinity) failed. The n_{Si}/n_{Al}-ratio of obtained materials was always constant. Further attempts were made to synthesize a SUZ-4 catalyst with boron instead of aluminum. However, without aluminum the synthesis did not result in any crystalline product. Upon aluminum-presence, the co-incorporation of boron and aluminum into the SZR framework occurred at n_{Si}/n_{Al}-ratios equivalent to those in the catalyst S0 (see catalyst S0B, Tab. 1).

Fig. 2

In the following part, we describe investigations on post-modified SUZ-4 catalysts. Desilication with NaOH resulted in sample S1Na, while the sample treated with the soft base K_2CO_3 was named S1K.The alkaline-treatments resulted in yields of 73 and 35% based on the initial amount for catalysts S1K and S1Na, respectively. For S1K, no significant changes in agglomeration or crystal shape are observed by SEM. In contrast, the harsh alkaline conditions applied to S1Na clearly broke the agglomeration of SUZ-4 crystals (see Fig. 2, middle panels). BET surface area and total pore volume increase with stronger alkaline-treatment from initially 360 m^2/g (for S0) over 380 to 440 m^2/g for S1K and S1Na, respectively (see Tab. 1). The determined mesopore volume (V_{meso}) equals to 0.1 cm^3/g for S0, 0.2 cm^3/g for S1K and 0.3 cm^3/g for S1Na. The increased BET surface area and mesopore volume can be explained by the removal or relocation of amorphous species and EFAl blocking the pores, as in the case of Ferrierite catalysts [25], and the introduction of a secondary, hierarchical pore system upon desilication [17]. While S1K has the same water content as the parent S0 (9%), the water content of S1Na is increased to 13%. This can either be attributed to the higher

BET surface area of the catalyst or to an increased polarity of the zeolite surface due to a higher number of Si-OH groups.

Acid dealumination resulted in the catalyst S2N. No visible changes of agglomeration or crystal shape compared to the parent S0 could be observed by SEM. Though the total pore volume increased the inner surface area reflected by the BET is (with 380 m^2/g) just slightly higher than in case of the parent catalyst S0 (see Tab. 1). In parallel, the water content of S2N is also slightly increased from 9 to 11% after dealumination.

The copper-exchanged catalyst S3Cu has a blueish color that is caused by Cu^{2+} ions exchanged into the micropores of the zeolite. No structural changes occurred and no indication of extra-framework bulk $Cu^{II}O$ particles could be found in powder XRD patterns of S3Cu (see Fig. 1). The copper loaded S3Cu catalyst was also investigated by backscattering electron detection (BSE) in order to see any formed $Cu^{II}O$ nanoparticles (see Fig. 2, bottom). As can be seen by comparing the SEM image (bottom, left) and the BSE-detector image (bottom, right) no bright spots are found and thus no visible nanoparticles of > 10 nm are present. The images of the synthesized S3Cu can for further proof be compared to a SUZ-4 material containing CuO nanoparticles as a result of multiple ion exchanges; see SI, Fig. S2). The copper exchanged catalyst S3Cu had the same water content as the parent S0.

Tab. 1

Summarizing, the SUZ-4 catalysts tend to crystallize in a small range of bulk n_{Si}/n_{Al}-ratios, independently of the used gel composition. X-ray diffraction proves that the applied post-modifications tend to reduce relative crystallinity and decrease the average crystal size. The co-incorporation of boron results in bigger crystals of higher relative crystallinity. SEM images showed that the directly synthesized catalysts are highly agglomerated and that these agglomerates can be broken upon applying harsh desilication. N_2-physisorption revealed an increasing BET surface area and mesopore volume upon alkaline-treatment and dealumination. The water content of SUZ-4 catalysts increased over proportionally after post-modification with base and/or acid. This indicates an enhanced hydrophilic character of the catalyst surface.

3.2. The chemical composition of the framework – EDX and ^{27}Al MAS NMR

The chemical composition of the catalysts was determined by EDX and is summarized in Tab. 1. The catalysts have low n_{Si}/n_{Al}-ratios <10 ranging from 6.6 for the parent S0 to 7.9 for the dealuminated S2N and up to 8.8 for the desilicated S1Na. The n_{Si}/n_{Al}-ratio of copper-exchanged S3Cu is 6.8 and thus comparable to the parent S0. The boron containing S0B has a n_{Si}/n_{Al}-ratio of 6.6. This means, it bears the same aluminum content as the parent catalyst S0 (independent of gel composition, see also section 3.1). The n_{Si}/n_{Al}-ratios obtained by EDX are, however, not representative for the acidity of the catalysts. From the literature, it is known that in SUZ-4 not all potassium is exchangeable for NH_4^+ and that in general not all aluminum must be incorporated in the framework.

Extra-framework aluminum (EFAl) species were previously observed on SUZ-4 by adsorption of CO as probe [8]. This aluminum does not contribute to the overall Brønsted acidity [26]. The different aluminum species are herein investigated by ^{27}Al MAS NMR spectroscopy and the EFAl is quantified by evaluating the respective peak intensities. Peaks of octahedral coordinated aluminum at 0 ppm (EFAl) and of tetrahedral framework aluminum (FAl) at 55.5 ppm are observed in the ^{27}Al MAS NMR spectra that can be found in Fig. S3 in the SI. All herein investigated catalysts show EFAl species. The amount of these species can, because of the short excitation pulses applied to fully hydrated catalysts, be estimated reasonably from the peak intensities in the ^{27}Al MAS NMR spectra. Their relative amounts account for the EFAl content and are tabulated (see Tab. 1). Consequently, the n_{Si}/n_{Al}-ratio obtained by EDX in Tab. 1 can be corrected taking into account the estimated EFAl amounts [14]. In a second step, it can also be corrected for charge-balancing counter ions, subtracting one charge per incorporated K^+-ion and two charges per incorporated Cu^{2+}-ion. This results in the "effective n_{Si}/n_{Al}-ratios" found in Tab. 1 and the corresponding theoretical acid site densities (t-ASD). However, the reported t-ASD value does not account for remaining uncertainties, in particular: 1) if present, copper might also be incorporated at single aluminum sites, whereby the second charge is compensated by another OH-group [5], and 2) also the EFAl species can act as counter cations [27] with unknown stoichiometry. The accuracy of the obtained t-ASD values and the nature of the EFAl species is elucidated through the investigation of acidity and will be addressed in the next section (3.3).

To reveal at which stage of the synthesis procedure the EFAl is formed, we investigated a SUZ-4 catalyst directly after NH_4-exchange without any further treatment. The ^{27}Al MAS NMR spectrum of the NH_4-SUZ-4 catalyst can be found in Fig. S4 in the SI and shows no peak at 0 ppm in a fully hydrated state. We furthermore proved the absence of EFAl by calculating the framework n_{Si}/n_{Al}-ratio of the catalyst from deconvolution of the ^{29}Si MAS NMR spectra (also in Fig. S4).

Evaluation of the peak intensities of Q4(2Al) and Q4(1Al) silicon nuclei according to Löwenstein's rule resulted in a n_{Si}/n_{Al}-ratio of 6.8. This is within the accuracy of the method equal to the value from EDX. Thus, after the synthesis no EFAl is present. However, a dealumination of SUZ-4 occurs when ammonia is burned off at 773 K respectively when activating the catalyst at similar temperatures. This might also be origin of EFAl species in other publications [8].

The n_{Al}/n_B ratio of directly synthesized boron containing catalyst S0B was determined by ICP to be 50. To investigate the nature of boron species in the S0B framework, the catalyst was investigated by means of ^{11}B MAS NMR and FT-IR spectroscopy (see SI, Fig. S5). The ^{11}B MAS NMR spectrum of catalyst S0B is dominated by a peak at -2.2 ppm, attributable to tetrahedral boron in the zeolite framework structure [18]. The incorporation can be supported by FT-IR spectroscopy of the dry sample (see Fig. S5, right). The spectrum shows a characteristic band located at 1390 cm^{-1} that is attributed to boron in zeolite frameworks [28]. Additionally, a band attributable to bridging Si(OH)Al-groups is to be found at 3610 cm^{-1}, supporting the co-incorporation of both aluminum and boron in the framework of S0B. Despite the small boron content determined by ICP, both FT-IR and ^{11}B MAS NMR spectroscopy give surprisingly strong peaks of boron incorporated in the SUZ-4 framework.

Alkaline-treated catalysts have varying exchange-degrees. While S1K has an exchange degree that is increased from 54% to 62%, S1Na has with 51% exchanged potassium ions a rather small value compared with S0. A possible explanation can be found in the fact that potassium is partially located in 8-MR pores, but also in 6-MR cages [7]. The high potassium content of S1Na can thus be explained by an over proportional amount of potassium ions located in cages that withstand the NaOH-treatment. Furthermore, S1Na has a total n_{Si}/n_{Al}-ratio of 8.8, which is close to the highest value published so far for the SUZ-4 framework (n_{Si}/n_{Al}-ratio 9, no information about ASD or exchange degree; see [10]).

Although acids such as HNO_3 or HCl are frequently used to remove EFAl species, surprisingly, the catalyst with the highest EFAl content and thus the strongest peak at 0 ppm is the acid-dealuminated S2N. This indicates that aluminum is released from the framework, however, not transported out of the pores. Comparable observation have been made after dealumination of other 8-MR pore zeolites like Ferrierite and A [14, 29], because pore ring sizes below 12-MR restrict the removal of EFAl species [19]. Thus, a diffusion limitation in the 10- and 8-MR pores of the SZR topology results in EFAl species observed by ^{27}Al MAS NMR at 0 ppm. One could argue that the EFAl is a result of a too harsh treatment with 15 M HNO_3. To exclude this, additional dealuminated catalysts apart from S2N were synthesized in lower HNO_3-concentrations (30 min in 1 M or 15 M HNO_3). These treatments increased the ASD of the catalysts but had little impact on catalyst properties and MTO performance. These treatments also resulted in EFAl contents of 9% and 11%

and are in the range of values obtained for S0 and S2N (6% and 15%, respectively, see Tab. 1). Therefore, the described EFAl appearance is not a result of a too harsh treatment but a significant finding for dealuminated SUZ-4 catalysts. EDX investigations show that additionally significant amounts of potassium have been removed from the framework of S2N. This results in the, to the best of our knowledge, highest published exchange degree of 84% reported so far for SUZ-4 catalysts. It should be noted in this respect that the extraordinary high value "75%" cited by Zholobenko et al. [9] is based on data by Lawton et al. [7] and is rather 1 - 3.3/5.4% ≈ 40% exchanged potassium. For comparison, the directly synthesized catalysts S0 and S0B show exchange degrees of 54 and 56% (n_K/n_{Al}-ratio of 0.46 and 0.44), respectively.

The copper presence in S3Cu does not prevent the measurement and quantification of the ^{27}Al MAS NMR spectra as demonstrated elsewhere for Cu-SSZ-13 of comparable n_{Cu}/n_{Al}-ratio [30], whereas in previous literature no peak at 0 ppm was observable [31]. On S3Cu we see a small peak at 0 ppm, accounting for 2% of the total aluminum. The reduced EFAl content compared with S0 can tentatively be explained by the exchange procedure in slightly acidic environment at a high pH ≈ 5.5 that results in aluminum removal and/or realumination. Peak broadening at 0 ppm due to paramagnetic copper cannot be excluded. However from comparing the t-ASD in Tab. 1 (0.4 mmol/g) with the ASD from ammonia loading discussed in the next section (0.38 mmol/g) it gets clear that this error is rather low in case of S3Cu.

Summarizing, the chemical composition alone gives a distorted picture of the ASD of the SUZ-4 catalyst, because EFAl species and counter ions are not taken into account. In an attempt to overcome these limitations, we performed an indirect approximation of ASD (t-ASD). All post-modified catalysts showed EFAl in a quantity of up to 15% of the total aluminum content for S2N. For the first time, we evidence the incorporation of boron into a SUZ-4 catalyst, accompanied by aluminum incorporation at identical n_{Si}/n_{Al}-ratio as for the parent SUZ-4. Thus, we conclude that the crystallization of the SUZ-4 framework crucially requires aluminum incorporation as balance for the potassium ions acting as structure directing agent.

3.3. The accessibility of acid sites – ^{1}H MAS NMR and FT-IR

The acidity of the catalysts was in addition to the indirectly obtained t-ASD also directly investigated by applying probe molecules and spectroscopic techniques. Thereby, different probe molecules were used to access the respective acid sites. The SZR framework restricts diffusion of spheres (up to 0.469 nm diameter) in the 10-MR channel (compare to MFI with 0.470 nm), so pyridine will have access to the 10-MR pore, but not to the 8-MR pores with 0.332 nm restrictions [6]. Both 10-MR and 8-MR pores, however, are accessible to ammonia. Thus, a combination of both probes allows conclusive remarks on the location of acid sites in the framework. We quantified the formed ammonium ions by ^{1}H MAS NMR spectroscopy and the pyridine adducts using the band intensities assigned to Brønsted and Lewis sites and measured by FT-IR spectroscopy. We will initially discuss the spectra of unloaded catalysts and then the accessibility for probes in the directly synthesized and post-modified catalysts.

In Fig. 3, ^{1}H MAS NMR spectra of dehydrated SUZ-4 catalysts are shown. The peaks can be assigned as follows: 1.8 ppm to surface Si-OH, 2.3 ppm mainly to the Al-OH of EFAl species, 3.8 ppm to Si(OH)Al groups and the broad feature at 5.6 ppm to disturbed Si(OH)Al groups [27, 32]. In Fig. 3 a, the spectrum of the parent catalyst S0 is shown. It is dominated by an intense peak at 2.3 ppm, reflecting the presence of significant amounts of Al-OH groups (as found in EFAl sites). Upon exposure to ammonia and subsequent desorption of surplus molecules, the peak at 3.8 ppm disappears and a new peak due to ammonium ions at 6.5 ppm appears [32]. This proves that all acid sites giving rise to the peak at 3.8 ppm formed ammonium ions. The ammonium peak intensity at 6.5 ppm is evaluated and results in the respective acid site density (NH_3-ASD, see Tab. 1). The ^{1}H MAS NMR spectrum of S3Cu is found in Fig. 3 b) and shows a broadening of the peak at 3.8 ppm due to dehydration and presence of paramagnetic copper ions. A direct quantitative evaluation of this spectrum is not possible. However, upon ammonia loading, a broad and quantifiable peak of ammonium ions at 6.5 ppm is formed. Furthermore, the peak of Al-OH groups at 2.3 ppm is significantly smaller than on S0, in accordance with the small EFAl content of S3Cu as determined by ^{27}Al MAS NMR spectroscopy (see section 3.2). This also supports that the EFAL is not completely NMR invisible due to nearby paramagnetic copper nuclei. In Fig. 3 c) the ^{1}H MAS NMR spectra of parent and desilicated catalysts S0, S1K, and S1Na are shown. Note the decreasing peak at 3.8 ppm from S1K to S1Na as a result of the decreased ASD upon desilication. This is accompanied by an increased amount of non-interacting Si-OH groups at 1.8 ppm. Note also the decreasing peak at 2.3 ppm corresponding to Al-OH groups, which can be explained by a decreased total quantity of EFAl (in accordance with the aluminum content by EDX) and/or condensation of EFAl Al-OH groups to the oxide. Both observations are in agreement with observations made for desilicated ZSM-22 zeolites [16, 17].

Fig. 3

FT-IR spectra of characteristic SUZ-4 catalysts are shown in Fig. 4. The acquired measurements are comparable to already published spectra [8, 9]. On the left panel, the region from 3800 to 3400 cm^{-1} is shown, with bands of Si-OH groups at 3740 cm^{-1}, Al-OH groups at 3650 cm^{-1}, and Si(OH)Al groups at 3610 cm^{-1}. The spectra of dehydrated catalysts S0 and S1Na are shown before and after loading pyridine and desorption of surplus probe molecules [33]. It can be pointed out that the Al-OH peak is intense on S0, but of much smaller intensity on S1Na. This reflects the smaller content of these hydroxyls on the EFAl species on S1Na. This finding is in agreement with ^{1}H and ^{27}Al MAS NMR spectroscopy as well as the reduced aluminum content found by EDX. The Al-OH band at 3650 cm^{-1} is maintained after loading pyridine onto S0. Some intensity at 3610 cm^{-1} is also maintained even after pyridine adsorption for S0. This can be explained by a hindered accessibility of pyridine to acid sites in the parent SUZ-4. In contrast, when the desilicated catalyst S1Na is loaded with pyridine, the band of Si(OH)Al groups at 3610 cm^{-1} vanishes completely. This is a result of the interaction between acidic Si(OH)Al groups and pyridine forming a pyridinium ion. The Al-OH band at 3650 cm^{-1} stays untouched. In the region from 1600 cm^{-1} to 1400 cm^{-1}, the bands of protonated pyridine at 1547 cm^{-1} and of Lewis-bound pyridine at 1455 cm^{-1} are found [8]. The Lewis ASD of S0 (0.10 mmol/g) could be determined from the FT-IR band at 1460 cm^{-1}. Of course, this Lewis-ASD value is restricted by the diameter of pyridine and accounts only for the Lewis acidity in 10-MR pores. Conversely, EFAl in 8-MR pores cannot be probed since the Lewis acid sites there cannot interact with pyridine. For S0, this supports together with the low Brønsted ASD detected by ammonia (NH_3-ASD, compared to the predicted t-ASD) the location of EFAl preferentially in 8-MR pores. These are then clogged by EFAl species and thus inaccessible. Because of the huge difference between approximated t-ASD and probed ASD, we propose that EFAl species are present as counter ions in both the 10-MR and 8-MR pores of S0 in significant amounts, explaining also the reduced accessibility of SUZ-4 in previous studies [8]. It is noteworthy that the pores of S0 are widely accessible for the N_2 molecule used in physisorption experiments and the differences in between the catalysts are rather low. Thus it seems more difficult for polar probes to overcome the clogged 8-MR pores of S0 than for the N_2 molecule.

Fig. 4

The parent catalyst S0 has a total accessible ASD of 0.49 and 0.23 mmol/g for ammonia and pyridine, respectively (see Tab. 1). These values are comparable to literature values of Brønsted ASD determined by propylamine-TPD (0.63 mmol/g [8]), pyridine-IR (0.2 mmol/g [8]), and NH_3-TPD (0.36 mmol/g [12]). The loading with pyridine of the parent S0 took approximately 45 min and thus longer than for other investigated catalysts. Such diffusion limitations were previously described for a comparable SUZ-4 [8]. By calculating the difference between the ASD for ammonia and pyridine, the acidity in (accessible) 8-MR pores can be estimated. For S0 the ASD in 8-MR pores is estimated as 0.49 – 0.23 = 0.26 mmol/g. A remarkable difference in between t-ASD and NH_3-ASD is observed, being in the range of 1.1 – 0.49 ≈ 0.6 mmol/g. This difference can be explained by inaccessible acid sites (blocked e.g. by aluminum counter ions) and shows the limits of the t-ASD approximation. The FT-IR band of SUZ-4 located at 3610 cm^{-1} has previously been deconvoluted into up to 5 components, whereof three are discussed in detail belonging to 10-, 8-, and 6-MR acid sites, respectively [9]. The deconvolution was based on the assumption that all SZR ring structures bear one distinct acid site (while no absolute ASD was determined by the authors). They concluded that 50% of the total present acid sites are located in the 10-MR pores (and 40 % in the 8-MR, respectively). We found for the parent S0 the ASD 0.49 mmol/g being accessible for ammonia and the ASD 0.23 mmol/g being accessible for pyridine. Assigning the first to total accessible ASD and the second value to ASD in 10-MR pores, parent S0 shows a similar relation as proposed by Zholobenko et al. [9].

Co-incorporation of boron in S0B results in a total ASD of 1.05 mmol/g determined by NH_3-loading via quantitative ^1H MAS NMR spectroscopy. This is twice the amount of S0 and fits the approximated t-ASD (1.1 mmol/g). The high ASD of S0B determined by NH_3-loading compared with S0 gets thereby only a contribution of bridging Si(OH)Al groups but none of Si(OH)B. The reason is that incorporated boron is not able to stabilize the NH_4^+ ion under the applied conditions [18]. Note that also the t-ASD was determined without taking into account boron. At least 0.68 mmol/g of acid sites are located in the 8-MR of S0B. Thus, EFAl species seem not to act as counter ions in significant amounts, since NH_3-ASD and t-ASD are close. However, it shall be mentioned that potassium coordination at boron sites cannot completely be ruled out and thus there is maybe some counter ionic EFAl located at the aluminum sites. In combination with the improved relative crystallinity of the sample, we conclude that the presence of boron during the synthesis and its co-incorporation is beneficial to stabilize the framework and to avoid pore blocking by amorphous or EFAl species. The accessible Lewis acidity (0.12 mmol/g) is in the range of S0 (0.10 mmol/g) as expected for the rather low boron content. Present EFAl (8% of aluminum) is located mainly in 8-MR pores where the pyridine probe cannot enter.

In the following, we will discuss the acid sites in post-modified catalysts. All these catalysts show an increased bulk n_{Si}/n_{Al}-ratio, a significant EFAl amount and higher acid site accessibility. The alkaline treated catalyst S1K has 0.80 (NH_3-ASD) of 1.1 mmol/g (t-ASD) acid sites accessible for ammonia and 0.46 mmol/g accessible for pyridine (see Tab. 1). This difference of 0.3 mmol/g must again be interpreted as inaccessible acid sites. The main outcome of the treatment with K_2CO_3 is the removal of species that restrict the pores of the SZR framework, as seen in case of Ferrierite [25]. This finding for the difference between t-ASD and NH_3-ASD is also supported by the Py-ASD of 0.46 mmol/g compared to 0.23 mmol/g for S0 (see Tab. 1). The rising EFAl quantity compared to S0 is a result of a light desilication and the higher potassium exchange degree. This is also reflected by a slightly increasing V_{meso} found in Tab. 1. For S1Na, the overall ASD decreases significantly. A similar decrease in ASD is observed on other 1-dimensional 10-MR pore catalysts like ZSM-22 [16, 17]. As on ZSM-22, this is on SUZ-4 accompanied by an increased amount of Si-OH groups and a higher water content as a result of the desilication. All theoretically estimated acid sites (t-ASD = 0.5 mmol/g) are accessible by ammonia (ASD = 0.47 mmol/g). Of the latter acid sites, 0.27 mmol/g are accessible for pyridine and thus located in the 10-MR pore. This indicates that EFAl species are not present as counter ions in significant amounts. The rising n_K/n_{Al}-ratio is a result of the potassium ions that are not exchangeable and entrapped in cages [7]. Whereas in case of pyridine loaded S1Na no FT-IR band at 1460 cm^{-1} attributable to Lewis sites is visible, the ASD of these sites is 0.25 mmol/g for S1K. Conclusively, EFAl species are on S1K located in 10-MR pores and in 10-MR/8-MR intersections and accessible to pyridine. On S1Na however, EFAl species are located in 8-MR and therefore not accessible for pyridine (taking into account the accuracy of the measurement: < 0.05 mmol/g Lewis ASD in 10-MR). Furthermore, less Al-OH groups are observed according to ^1H MAS NMR and FT-IR spectroscopy. While the difference in between t-ASD and NH_3-ASD (both see Tab. 1) decreases for the SUZ-4 catalysts S0, S1K and S1Na from 0.6 to 0.3 and finally to ≈ 0 mmol/g, the relative amount of EFAl species increases from 6 to 8 to 11% for the respective catalysts. In the same order the BET surface area increased from 360 over 380 to finally 440 m^2/g. Summarizing a desilication makes the pores and acid sites of SUZ-4 better accessible for probes. This is due to the introduced of an hierarchical pore system and less pore blockings.

Dealuminated S2N has to our knowledge both the highest potassium exchange degree (84%) and NH_3-ASD (1.12 mmol/g, see Tab. 1) that has been reported so far for SUZ-4. The removal of aluminum through dealumination of SUZ-4 is compensated by new acid sites formed through the exchange of potassium. Most acid sites on S2N predicted by indirect techniques (t-ASD of 1.3 mmol/g) are accessible to ammonia (1.12 mmol/g). Thus fewer EFAl species can act as counter ions and as a result of the exchange degree the ASD in 8-MR pores is 0.8 mmol/g and thus twice the amount of S0. Also the Brønsted and Lewis ASD (0.33 and 0.24 mmol/g) probed by pyridine are high. Conclusively,

the accessibility of all pores for polar probes has increased dramatically after dealumination compared with the parent S0. Because of the increase in Lewis acidity, EFAl (15% of total aluminum) seems to be present in both 10- and 8-MR pores.

The copper exchanged S3Cu has a total acidity of 0.38 mmol/g. This reflects remarkably the value approximated as t-ASD (0.4 mmol/g) and thus supports that Cu^{2+} ions compensate approximately two acid sites each. The few detected EFAl species do not act as counter ions. The pyridine loading of S3Cu results in a Brønsted ASD of 0.27 mmol/g in the 10-MR pores. This is comparable to the parent S0, even though for this catalyst a lot of acid sites were not accessible. The Lewis acidity of S3Cu is 0.43 mmol/g and thus far greater than for S0 (0.10 mmol/g). In section 3.2 it was shown that the n_K/n_{Al}-ratio of S3Cu was slightly reduced and EFAl acting as counter ions on S0 were removed during the copper exchange at pH < 6. This suggests that the EFAl was replaced by another counter ion like copper. Likewise, the low Brønsted ASD in the 8-MR pores and the few exchanged potassium ions indicate that the Cu^{2+} ions cannot be primary located in the 8-MR pores. Conclusively, the introduced copper ions are most reasonably located in the for pyridine accessible 10-MR pore or in 10-MR/8-MR intersections, supported by *operando* XAS measurements (see Section 3.4.1). This explains the increased Lewis acidity determined from pyridine loadings.

To summarize this section, the loading with different probe molecules proved that the accessibility of the 8- and 10-MR pores in the framework is depending on the treatment. The difference in between t-ASD and NH_3-ASD was proven to be a valuable indicator of the accessibility. Respective ASDs in both 10- and 8-MR pores could be calculated from the measurements. In the parent S0 the EFAl is most likely acting as counter ion, whereas this is to a smaller extent the case for the post-modified samples. In the desilicated sample S1Na, the octahedral EFAl is inaccessible to pyridine and thus most likely located in 8-MR pores.

3.4. Catalytic performance of the SUZ-4 catalysts

3.4.1. Methanol-to-olefin (MTO) conversion

The SUZ-4 materials were evaluated in the methanol-to-olefins (MTO) conversion. Different weight hourly space velocities (WHSV) of 0.5 and 0.2 ($g_{MeOH}g_{Catalyst}^{-1}$)$h^{-1}$ at 673 K were employed in order to study the effect of post-treatments on the performance of the materials. In a previous study, a WHSV of 2 h^{-1} led within few minutes to the deactivation of SZR zeolites [8]. At a WHSV = 0.5 h^{-1}, the herein shown SUZ-4 catalysts deactivate from an initial conversion of 100% to 20% within 2 h on stream (not shown). Although the modified catalysts (especially S1Na) exhibit slightly prolonged lifetime, a lower WHSV (here 0.2 h^{-1}) enables a more accurate description of the impact of post-modifications on the lifetime of the materials, as depicted in Fig. 6.

Fig. 5

Clearly, the parent material S0 exhibits the fastest deactivation under the applied conditions. Modified catalysts S2N, S1K, and S0B show a relatively similar deactivation behavior but outperform the parent by 30-60 min time on stream (TOS). A doubled lifetime compared to S0 is observed for the desilicated S1Na, whose deactivation is more gradual than for the other catalysts. It has also the smallest coke content (8%) of the investigated catalysts, however, it is higher than for other 10-MR structures, like ZSM-22 catalysts (<4%, see [34]). The catalysts show total methanol conversion capacities reaching from 0.4 to 0.8 g_{MeOH}/g_{Cat}. From these values, one can calculate the selectivity to coke. For S0 the selectivity to coke is 3 % (see Tab. 1) whereas in best case for S1Na the total selectivity to coke is 1% of feed methanol. The conversion capacity of the SUZ-4 catalysts correlates with the BET surface area, as evidenced by Fig. S7 in the SI. This supports that SUZ-4 catalysts applied in the MTO conversion are not limited by their available ASD as for example ZSM-5 catalysts, but by the accessibility of the pore system. A correlation between the conversion capacity of the SUZ-4 catalysts and the selectivities (C_5 – C_6 range products, ethene, propene) or the ASD in different parts of the pore system gave no meaningful results, also because of the limited amount of data points.

The selectivities to olefins during the MTO conversion are plotted in Figs. S6. All catalysts yield a significant amount of short alkenes and alkanes. In accordance with the temperature-dependent measurements performed by Teketel et al. [8], also herein investigated SUZ-4 catalysts produce at 673 K mainly short alkenes like ethene, propene and alkanes. This points to a low contribution from the aromatic-based reaction cycle as in 8-MR and some 10-MR catalysts [2].

Initially, a C_3 yield over 40% can be observed, whereas the C_2 yield is around 20%. The aromatics yield is for all the herein investigated catalysts below 5%. Especially catalyst S1Na shows a rather constant C_5-C_6 yield. This can be assigned to the high accessibility of the framework, including its mesopores, in combination with the rather low ASD that makes cracking of the long-chain products less probable [8, 17]. Even fewer aromatics were reported at 673 K and WHSV = 2 h^{-1} using the SZR structure [8], probably a result of the smaller residence time of molecules in the catalyst compared to our data.

Summarizing reflecting the characterization, the post-modified catalysts show a longer lifetime than S0. This might be the case because 10-MR and 8-MR pores are to a lesser extent blocked by counter ions like potassium and EFAl species. The mesoporous S1Na has a doubled lifetime compared to S0 and it shows during deactivation an elongated S-shaped conversion-TOS plot, as similarly observed for 10-MR catalysts of low ASD [34]. S1Na shows additionally a higher selectivity to aromatics (up to 7% after 1 h TOS, comparable S1K) and C_5+C_6 aliphatics. This can be explained by a growing influence of the now better accessible 10-MR channel on the product distribution, enabling long molecules and aromatics to leave the zeolite pores. The low ASD of the catalyst prevents thereby the cracking of C_5+C_6 aliphatics. Since the straight 10-MR pore is running parallel to the SUZ-4 needle main axis, few 10-MR pore openings and many 8-MR pore openings are present. Necessarily, a significant part of the diffusion will still happen through the 8-MR channels. These however are small and tend to get blocked by counter ions and coke. Thus, the deactivation rate of SUZ-4 in the MTO conversion is high compared to other catalysts.

3.4.2. Methane-to-methanol conversion

After copper ion exchange S3Cu was investigated in the stepwise methane-to-methanol conversion. The conversion sequence consists of the catalyst activation in oxygen, the loading with methane and the steam-assisted methanol extraction. During the high temperature activation step in the presence of O_2, the formation of active Cu_xO_y species within the zeolite pores occurs [5]. SUZ-4 was proven to be active in this reaction [4] and can furthermore be compared to the structurally related CHA catalysts [24] (see Tab. 2).

Tab. 2

The main product of the extraction step is methanol and the normalized productivity is 16.4 $mmol_{CH3OH}/mol_{Cu}$. This is more than for a recently published Cu,Na-SUZ-4 catalyst yielding 11.5 $mmol_{CH3OH}/mol_{Cu}$[4]. Over S3Cu also overoxidation products in the form of CO_x species were observed (~5.1 $mmol_{CH3OH}/mol_{Cu}$). The increased productivity compared to the literature value can be explained by the use of proton instead of sodium counter ions as well as the different reaction conditions [35]. However, it must in this respect be pointed out that other zeolite frameworks show a greater total productivity. For example, herein we included a Cu,H-SSZ-13 zeolite from our recent study [24] with a n_{Cu}/n_{Al}-ratio comparable to S3Cu. This zeolite yields under identical conditions 96.5 $mmol_{CH3OH}/mol_{Cu}$ of methanol, but also more overoxidation products (16 $mmol_{COx}/mol_{Cu}$). The Cu-SUZ-4 catalyst is thus outperformed by other catalysts by almost factor 9 and the question why this is the case is discussed in the following paragraphs.

Fig. 6

In order to investigate the state of copper in S3Cu during the methane-to-methanol conversion, *operando* XAS was employed. The X-ray absorption near edge structure (XANES) and the extended X-ray absorption fine structure (EXAFS) spectra are shown in Fig. 5 left and right panel, measured after stabilization of the system at each step. The O_2-activated form of the catalyst, after pretreatment at 727 K (red line), reveals a dominant Cu^{II} oxidation state as indicated from characteristic XANES features. The shoulder in the rising edge in the 8985–8990 eV range is assigned to 1s → 4p transitions of Cu^{II} while the weak pre-edge peak is assigned to the dipole forbidden 1s →

3d transition in d^9 Cu^{II} ions. Within the spectral resolution of our data, no evidence of Cu^{I} species was found. They would result in a well-defined rising-edge peak at energies below 8984 eV. The phase-uncorrected FT-EXAFS spectra (k^2-weighted) reveal three defined maxima at 1.4 Å., 2.35 Å and 3.2 Å. Especially the second shell peak can be correlated, according to previous studies [36, 37], to the strong coordination of Cu with the framework. The intensities of both the first and second shell peaks for O_2-activated S3Cu is similar to what has been observed for Cu^{II} species in paired, so-called 2Al sites (= Al-Si-Al or Al-Si-Si-Al motif) in the 6-MR of CHA frameworks [24, 37, 38]. These sites are known for having a remarkable stability against aging [30]. The third maximum in the FT-EXAFS spectra, also observed for Cu-CHA catalysts [31], can be tentatively associated with long-range Cu-Cu scattering paths in multimeric Cu_xO_y species, accounting for a minor fraction of the copper present in the material.

In the second reaction step after helium flushing, methane was loaded at a reaction temperature of 473 K. The XANES spectra obtained after stabilization show an incremented amount of Cu^{I} species. This is a result of the reduction to Cu^{I} upon forming a methoxy group, as it was similarly observed in the case of Cu-MOR [39, 40] and Cu-CHA [24]. The FT-EXAFS spectra reveal only minor changes in the intensity of the 1st coordination shell and 2nd coordination shell due to the weak interaction of CH_4 species with Cu and/or due to the low abundance of active copper sites. This results in the low productivity of S3Cu towards methanol.

During the last step, the steam-assisted methanol extraction, the XANES reveals a reoxidation of the Cu^{I} species to Cu^{II} indicated by the decrease of the rising edge peak at 8984 eV assigned to the 1s → 4p transition of Cu^{I}. Nonetheless, at the end of the steam assisted methanol extraction step the initial state of the catalyst is not restored since some Cu^{I} species remain observable. The copper species undergoing this re-oxidation after methanol extraction have been suggested to be the active ones for the methane conversion [24]. A partial hydration of the copper sites in the catalyst during extraction is evidenced by the increased intensity of the white line, reflecting the increased coordination of copper in the hydrated state. In addition, a decrease of the second shell peak is observed. This is consistent with a water induced mobilization (=detachment) of copper from their positions in close interaction with the zeolite framework.

Generally, a fraction of the copper ions present in SUZ-4 is redox active, as evidenced from characteristic features of XANES that change during the different process steps. However, also a strong coordination of copper to the zeolite framework along the whole sequence is evident. The 6-MR structures in the 10-MR next to the 8-MR entrance is postulated as the preferential location of copper ions. This structural motif is located below the 6-MR cages of the SZR structure that bear some not exchangeable potassium ions [6]. We conclude this because, first, potassium is widely

remaining in the 8-MR pores and blocking them also after copper exchange (see Tab. 1). Second, a similar 2Al site location of inactive copper ions in 6-MR exists in Cu-CHA catalysts [24, 37, 38]. This is supported by the fact that Cu^{II} balances two deprotonated Si(OH)Al sites, which agrees with the discussion in section 3.3: the comparison of t-ASD and NH_3-ASD led to the conclusion that each Cu^{II} approximately compensates two acid sites in SUZ-4. Given the high Al content of SUZ-4, the strong coordination of copper ions to the framework, and the low methanol productivity, it is conclusive that on SUZ-4 a similar 2Al location in 6-MR can be assumed. Finally, S3Cu has an increased Lewis ASD compared to the parent S0. This can be seen as a result of the interaction of pyridine with copper. Thus, pyridine must be able to access the copper in the 10-MR. Summarizing, we conclude that the strong coordination environment of Cu^{II} in the 6-MR of the SUZ-4 main channel hinders the formation of active sites, explaining the poor activity of S3Cu in the methane-to-methanol conversion.

4. Conclusion

All herein reported new SUZ-4 catalysts show an improved accessibility of pores and acid sites and as result a better reactivity in methane respective methanol conversions compared to already published ones. Extra-framework (EFAl) species are formed in the SUZ-4 framework upon burning off the ammonia. By comparing the acid site densities (ASD) determined by using ammonia and pyridine as probe molecules, we could measure the ASD located in the 10-MR and 8-MR catalyst pores. By comparing with the theoretically expected ASD we evaluated the overall accessibility of the catalyst. The presented procedure can in future be helpful to understand the reactivity of not completely accessible zeolite systems with multiple pore sizes.

EFAl formation and remaining potassium counter ions result in a partial blocking of 8- and 10-MR pores. Through a direct synthesis, it was possible to co-incorporate boron with aluminum into the SUZ-4 framework. Boron presence resulted in a better accessibility of pores and acid sites and in an increased relative crystallinity. Gel aging resulted in SUZ-4 crystals in the shape of elongated needles in dumbbell-like agglomeration, but same composition. All post-modifications (desilication and dealumination) increased the BET surface area and resulted in a reduced average crystal size. Alkaline treatments increased the content of Si-OH groups while decreasing the relative crystallinity. Thereby, soft alkaline treatment increased the BET surface area to 380 m^2/g and the ASD in 10-MR and 8-MR pores. Strong desilication with NaOH resulted in a reduced total ASD of 0.47 mmol/g with n_{Si}/n_{Al}-ratio 8.8 and in the highest BET surface area of 440 m^2/g. The indirectly determined theoretical ASD was completely accessible. Dealumination yielded a high extra-framework (EFAl) content of 15% and the highest ASD of 1.12 mmol/g as result of the potassium exchange degree of 84%. All improved catalysts outperformed the parent SUZ-4 in the methanol-to-olefin conversion (MTO). The desilication of the framework doubled the lifetime while the selectivity to short alkenes and alkanes was high. However a fast coke accumulation deactivated the catalysts. Copper containing SUZ-4 showed a lower activity in the methane-to-methanol oxidation compared to CHA catalysts. *Operando* XAS studies and indirect measurements revealed that the majority of copper is tightly coordinated as Cu^{II} in 2Al sites located in 6-MR motifs of the SZR 10-MR pore and not reactive.

Acknowledgements

This publication forms a part of the iCSI (industrial Catalysis Science and Innovation) Centre for Research-based Innovation, which receives financial support from the Research Council of Norway under contract no. 237922.

M.D. thanks D. Wragg for most valuable discussions on the XRD patterns. The authors want to thank all the colleagues that helped out during the measurements at the ESRF, namely C. Lamberti, K. A. Lomachenko and I. A. Pankin as well as A. Longo from BM26A at the ESRF.

References

[1] J. Weitkamp, Zeolites and catalysis, S. S. Ionics, 131 (2000) 175-188.
[2] U. Olsbye, S. Svelle, M. Bjorgen, P. Beato, T.V. Janssens, F. Joensen, S. Bordiga, K.P. Lillerud, Conversion of methanol to hydrocarbons: how zeolite cavity and pore size controls product selectivity, Angew. Chem. Int. Ed., 51 (2012) 5810-5831.
[3] F.J. Keil, Methanol-to-hydrocarbons: process technology, Microp. Mesop. Mater., 29 (1999) 49-66.
[4] M.B. Park, S.H. Ahn, A. Mansouri, M. Ranocchiari, J.A. van Bokhoven, Comparative study of diverse copper zeolites for the conversion of methane into methanol, ChemCatChem, (2017).
[5] P.J. Smeets, M.H. Groothaert, R.A. Schoonheydt, Cu based zeolites: A UV–vis study of the active site in the selective methane oxidation at low temperatures, Catal. Tod., 110 (2005) 303-309.
[6] C. Baerlocher, L.B. McCusker, Database of zeolite structures, http://www.iza-structure.org/databases/, accessed 10.08.2017.
[7] S.L. Lawton, J.M. Bennett, J.L. Schlenker, M.K. Rubin, Synthesis and proposed framework topology of zeolite SUZ-4, J. Chem. Soc. Chem. Comm., (1993) 894-896.
[8] S. Teketel, L.F. Lundegaard, W. Skistad, S.M. Chavan, U. Olsbye, K.P. Lillerud, P. Beato, S. Svelle, Morphology-induced shape selectivity in zeolite catalysis, J. Catal., 327 (2015) 22-32.
[9] V.L. Zholobenko, L.D. B., D. J., W.J. Smith, Ferrierite and SUZ-4 zeolite: characterization of acid sites, J. Phys. Chem. B, 102 (1998) 2715-2721.
[10] S. Gao, X. Wang, X. Wang, Y. Bai, Green synthesis of SUZ-4 zeolite controllable in morphology and SiO2/Al2O3 ratio, Microp. Mesop. Mater., 174 (2013) 108-116.
[11] S. Gao, X. Wang, M. Li, X. Wang, J. Li, J. Feng, Nanofibrous SUZ-4 loading Pt used for selective catalytic reduction of NOx by hydrogen, Microp. Mesop. Mater., 183 (2014) 185-191.
[12] N. Katada, K. Suzuki, T. Noda, M.B. Park, H.-K. Min, S.B. Hong, M. Niwa, Ammonia IRMS-TPD characterization of Brønsted acid sites in medium-pore zeolites with different framework topologies, Top. Catal., 53 (2010) 664-671.
[13] A.C. Gujar, A.A. Moye, P.A. Coghill, D.C. Teeters, K.P. Roberts, G.L. Price, Raman investigation of the SUZ-4 zeolite, Microp. Mesop. Mater., 78 (2005) 131-137.
[14] M. Müller, G. Harvey, R. Prins, Comparison of the dealumination of zeolites beta, mordenite, ZSM-5 and ferrierite by thermal treatment, leaching with oxalic acid and treatment with SiCl4 by 1H, 29Si and 27Al MAS NMR, Microp. Mesop. Mater., 34 (2000) 135-147.
[15] Y. Oumi, S. Nemoto, S. Nawata, T. Fukushima, T. Teranishi, T. Sano, Effect of the framework structure on the dealumination–realumination behavior of zeolite, Mater. Chem. Phys., 78 (2002) 551-557.
[16] P. del Campo, P. Beato, F. Rey, M.T. Navarro, U. Olsbye, K.P. Lillerud, S. Svelle, Influence of post-synthetic modifications on the composition, acidity and textural properties of ZSM-22 zeolite, Catal. Tod., 299 (2017) 120-134.
[17] M. Dyballa, U. Obenaus, M. Rosenberger, A. Fischer, H. Jakob, E. Klemm, M. Hunger, Post-synthetic improvement of H-ZSM-22 zeolites for the methanol-to-olefin conversion, Microp. Mesop. Mater., 233 (2016) 26-30.
[18] V.R.R. Marthala, W. Wang, J. Jiao, Y. Jiang, J. Huang, M. Hunger, Effect of probe molecules with different proton affinities on the coordination of boron atoms in dehydrated zeolite H-[B]ZSM-5, Microp. Mesop. Mater., 99 (2007) 91-97.
[19] S.I. Zones, A. Benin, S.J. Hwang, D. Xie, S. Elomari, M.F. Hsieh, Studies of aluminum reinsertion into borosilicate zeolites with intersecting channels of 10- and 12-ring channel systems, J. Am. Chem. Soc., 136 (2014) 1462-1471.
[20] A. Auroux, Acidity and Basicity: determination by adsorption microcalorimetry, in: H.G. Karge, J. Weitkamp (Eds.) Molec. Sieves: Sci. Technol., Springer, Berlin Heidelberg, 2008, pp. 69.
[21] D. Massiot, F. Fayon, M. Capron, I. King, S. Le Calvé, B. Alonso, J.-O. Durand, B. Bujoli, Z. Gan, G. Hoatson, Modelling one- and two-dimensional solid-state NMR spectra, Magn. Reson. Chem., 40 (2002) 70-76.
[22] D. Bellet, B. Gorges, A. Dallery, P. Bernard, E. Pereiro, J. Baruchel, A 1300 K furnace for in situ X-ray microtomography, J. Appl. Crystall., 36 (2003) 366-367.

[23] B. Ravel, M. Newville, ATHENA, ARTEMIS, HEPHAESTUS: data analysis for X-ray absorption spectroscopy using IFEFFIT, J. Synchrotron Rad., 12 (2005) 537-541.
[24] D.K. Pappas, E. Borfecchia, M. Dyballa, I. Pankin, K.A. Lomachenko, A. Martini, M. Signorile, S. Teketel, B. Arstad, G. Berlier, C. Lamberti, S. Bordiga, U. Olsbye, K.P. Lillerud, S. Svelle, P. Beato, Methane to methanol: structure-activity relationships for Cu-CHA, J. Am. Chem. Soc., 139 (2017) 14961-14975.
[25] V.R.R. Marthala, M. Hunger, F. Kettner, H. Krautscheid, C. Chmelik, J.r. Kärger, J. Weitkamp, Solvothermal synthesis and characterization of large-crystal all-silica, aluminum-, and boron-containing Ferrierite zeolites, Chem. Mater., 23 (2011) 2521-2528.
[26] D. Freude, T. Fröhlich, M. Hunger, H. Pfeiffer, G. Scheler, NMR studies concerning the dehydroxylation of zeolites HY, Chem. Phys. Lett., 98 (1983) 263-266.
[27] M. Hunger, Multinuclear solid-state NMR studies of acidic and non-acidic hydroxyl protons in zeolites, Solid State Nucl. Magn. Reson., 6 (1996) 1-29.
[28] D. Scarano, A. Zecchina, S. Bordiga, F. Geobaldo, G. Spoto, G. Petrini, G. Leofanti, M. Padovan, G. Tozzola, Fourier-transform infrared and raman spectra of pure and Al-, B-, Ti- and Fe-substituted silicalites: Stretching-mode Region, J. Chem. Soc. Faraday Trans., 89 (1993) 4123-4130.
[29] M. Dyballa, U. Obenaus, S. Lang, B. Gehring, Y. Traa, H. Koller, M. Hunger, Brønsted sites and structural stabilization effect of acidic low-silica zeolite A prepared by partial ammonium exchange, Microp. Mesop. Mater., 212 (2015) 110-116.
[30] S. Prodinger, M.A. Derewinski, Y. Wang, N.M. Washton, E.D. Walter, J. Szanyi, F. Gao, Y. Wang, C.H.F. Peden, Sub-micron Cu/SSZ-13: Synthesis and application as selective catalytic reduction (SCR) catalysts, Appl. Cat. B: Env., 201 (2017) 461-469.
[31] J. Palamara, K. Seidel, A. Moini, S. Prasad, Ion distribution in copper exchanged zeolites by using Si-29 spin lattice relaxation analysis, J. Magn. Reson., 267 (2016) 9-14.
[32] Y. Jiang, J. Huang, W. Dai, M. Hunger, Solid-state nuclear magnetic resonance investigations of the nature, property, and activity of acid sites on solid catalysts, Solid State Nucl. Magn. Reson., 39 (2011) 116-141.
[33] L.M. Kustov, V.B. Kazansky, S. Beran, L. Kubelkova, P. Jiru, Adsorption of carbon monoxide on ZSM-5 zeolites. Infrared spectroscopic study and quantum-chemical calculations, J. Phys. Chem., 91 (1987) 5247-5251.
[34] M. Dyballa, P. Becker, D. Trefz, E. Klemm, A. Fischer, H. Jakob, M. Hunger, Parameters influencing the selectivity to propene in the MTO conversion on 10-ring zeolites: directly synthesized zeolites ZSM-5, ZSM-11, and ZSM-22, Appl. Catal. A: Gen., 510 (2016) 233-243.
[35] S. Grundner, W. Luo, M. Sanchez-Sanchez, J.A. Lercher, Synthesis of single-site copper catalysts for methane partial oxidation, Chem. Comm., 52 (2016) 2553-2556.
[36] K.A. Lomachenko, E. Borfecchia, C. Negri, G. Berlier, C. Lamberti, P. Beato, H. Falsig, S. Bordiga, The Cu-CHA deNOx catalyst in action: Temperature-dependent NH3-assisted selective catalytic reduction monitored by operando XAS and XES, J. Am. Chem. Soc., 138 (2016) 12025-12028.
[37] C. Paolucci, A.A. Parekh, I. Khurana, J.R. Di Iorio, H. Li, J.D. Albarracin Caballero, A.J. Shih, T. Anggara, W.N. Delgass, J.T. Miller, F.H. Ribeiro, R. Gounder, W.F. Schneider, Catalysis in a cage: condition-dependent speciation and dynamics of exchanged Cu cations in SSZ-13 zeolites, J. Am. Chem. Soc., 138 (2016) 6028-6048.
[38] E. Borfecchia, K.A. Lomachenko, F. Giordanino, H. Falsig, P. Beato, A.V. Soldatov, S. Bordiga, C. Lamberti, Revisiting the nature of Cu sites in the activated Cu-SSZ-13 catalyst for SCR reaction, Chem. Sci., 6 (2015) 548-563.
[39] E.M.C. Alayon, M. Nachtegaal, A. Bodi, J.A. van Bokhoven, Reaction conditions of methane-to-methanol conversion affect the structure of active copper sites, ACS Catal., 4 (2013) 16-22.
[40] V.L. Sushkevich, D. Palagin, M. Ranocchiari, J.A. van Bokhoven, Selective anaerobic oxidation of methane enables direct synthesis of methanol, Science, 356 (2017) 523-527.

Tables

Table 1: Summary of SUZ-4 catalyst properties.

	S0	S0B	S1K	S1Na	S2N	S3Cu
Yield [%]	-	-	73	35	67	100
Relative crystallinity [%][1]	90	95	90	80	90	90
Average crystallite size [nm][1]	37	41	33	31	34	34
BET [m^2/g]	360	360	380	440	380	360
V_{tot} [cm^3/g]	0.3	0.3	0.3	0.4	0.4	0.3
V_{meso} [cm^3/g]	0.1	0.1	0.2	0.3	0.2	0.2
Water content [%]	9	8	9	13	11	9
n_{Si}/n_{Al}-ratio[2]	6.6	6.6	7.2	8.8	7.9	6.8
n_{Al}/n_{B}-ratio[3]	-	50	-	-	-	-
n_{Cu}/n_{Al}-ratio[2]	-	-	-	-	-	0.18
n_{K}/n_{Al}-ratio[2]	0.46	0.44	0.38	0.59	0.16	0.41
EFAl [%][4]	6	8	9	11	15	2
Effective n_{Si}/n_{Al} ratio[5]	7 (15)	7 (15)	8 (14)	10 (32)	10 (13)	7 (36)
Theoretical t-ASD [mmol/g][6]	1.1	1.1	1.1	0.5	1.3	0.4
NH_3-ASD [mmol/g][7]	0.49	1.05	0.80	0.47	1.12	0.38
Inaccessible ASD [mmol/g][8]	0.60	unknown	0.30	< 0.1	0.18	< 0.1
Py-ASD [mmol/g][9]	0.23	0.37	0.46	0.27	0.33	0.27
Lewis Py-ASD [mmol/g][9]	0.10	0.12	0.25	< 0.05*	0.24	0.43
Coke after MTO [%]	10	10	10	8	10	-
Conversion capacity [g_{MeOH}/g_{Cat}]	0.40	0.60	0.58	0.80	0.50	-

1 from X-ray diffraction (accuracy ±5)

2 calculated from EDX

3 from ICP - OES

4 extra framework aluminum content according to ^{27}Al MAS NMR spectroscopy

5 framework n_{Si}/n_{Al} ratio corrected for the EFAl (in parentheses: additionally corrected for K^+ and Cu^{2+})

6 calculated from the framework n_{Si}/n_{Al} ratios and corrected for counter ions (annotation 5)

7 quantitative ^{1}H MAS NMR spectroscopy after ammonia loading (accuracy ± 10%)

8 difference of t-ASD (annotation 6) and NH_3-ASD (annotation 7)

9 quantitative FT-IR spectroscopy after pyridine loading (accuracy ± 15%)

*no band at 1455 cm^{-1} quantifiable

Table 2: Comparison of the methane oxidation capacity of S3Cu (n_{Si}/n_{Al}-ratio 6.8 and n_{Cu}/n_{Al}-ratio 0.18) compared with literature catalysts. The CHA sample (Cu,H-SSZ-13 catalyst with n_{Si}/n_{Al}-ratio 12 and n_{Cu}/n_{Al}-ratio 0.16 [24]) was activated comparative to S3Cu (8 h / 773 K). The SZR sample (Cu,Na-SUZ-4 catalyst with n_{Si}/n_{Al}-ratio 8.2 and n_{Cu}/n_{Al} ratio 0.43 [4]) was activated shorter in O_2 (4 h / 723 K).

Sample	Copper [wt%]	Methanol [mmol/mol Cu]	CO_x [mmol/mol Cu]	Reference
S3Cu	2.4	16.4	5.1	this work
CHA	1.4	96.5	16	[24]
SZR	4.3	11.5	unknown	[4]

Figure captions

Figure 1: Powder X-ray diffraction patterns (XRD) of the SUZ-4 catalysts investigated in this contribution. Reflection peaks belong to the SZR structure type as expected for SUZ-4.

Figure 2: SEM pictures of representative catalysts showing (from top to bottom) the agglomeration and crystal shape of parent SUZ-4 S0, the broken agglomerates after desilication with NaOH (S1Na) and a backscattering electron (BSE) image of S3Cu. Absence of bright spots proves that no nanoparticles > 10 nm have formed.

Figure 3: ^{1}H MAS NMR spectra of dehydrated SUZ-4 catalysts. The ammonia loading of S0 and S3Cu in a) and b) leads to a shift and intensity change as a result of ammonium ion formation and the corresponding peak at 6.5 ppm. The evolution of ^{1}H MAS NMR spectra after alkaline treatment (S1K, S1Na) and the increased number of Si-OH groups with their peak at 1.8 ppm is shown in c).

Figure 4: FT-IR spectra of S0 and S1Na. Left the OH-group region in between 3800 and 3400 cm^{-1} of dried and pyridine loaded (+Py) catalysts showing bands of Si-OH, Al-OH and Si(OH)Al groups. Right the region in between 1600 cm^{-1} and 1400 cm^{-1} with bands ascribed to Brønsted (1547 cm^{-1}) and Lewis (1455 cm^{-1}) acid site bound pyridine, respectively.

Figure 5: Catalytic data of directly synthesized (circles), alkaline treated (triangles) and dealuminated (rectangles) SUZ-4 catalysts applied in the MTO conversion, plotted as methanol conversion *X* against TOS (WHSV = 0.2 h^{-1}, *T* = 673 K).

Figure 6: *Operando* XAS measurements on S3Cu showing the Kα-edge of Cu (left) and the EXAFS region (right) of the four reaction steps: Methane oxidation in oxygen (red), a following He flush (dotted black), reaction with methane (green) and water introduction with He-wet (blue).

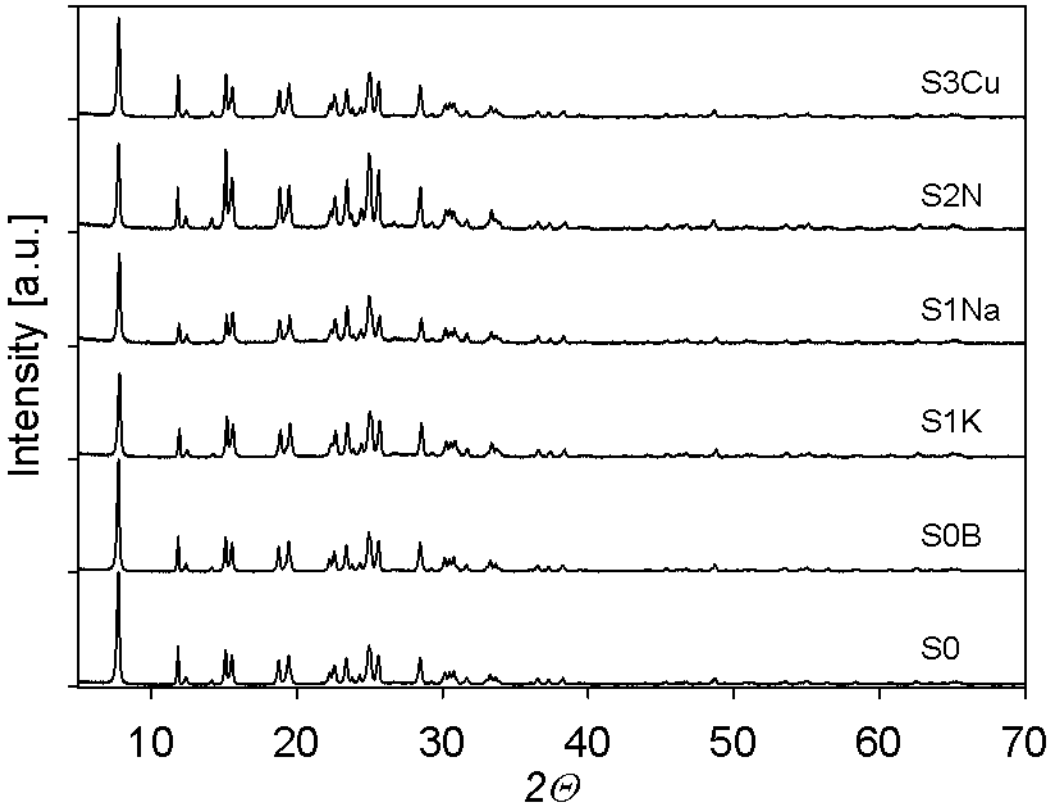

Fig. 1

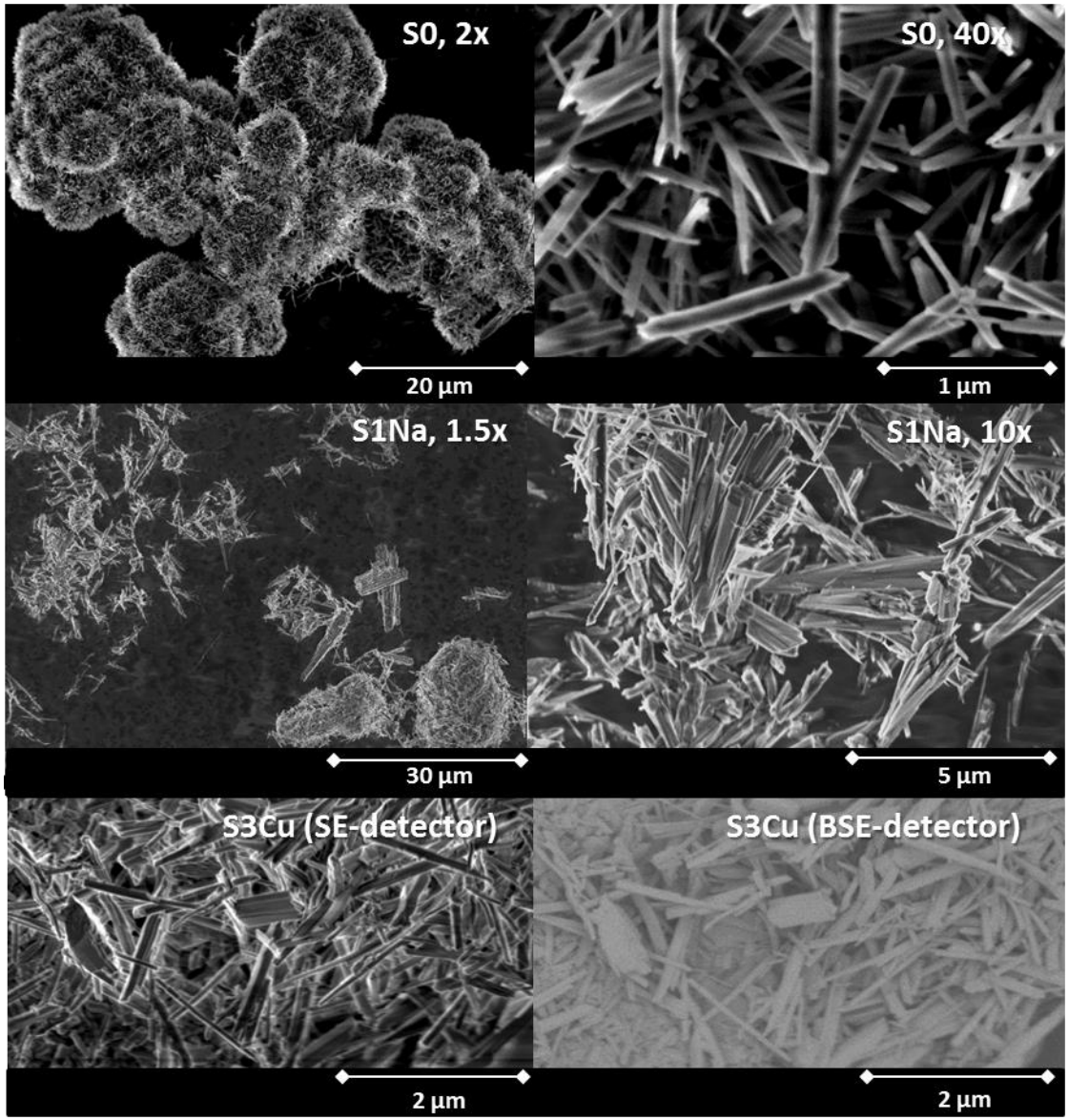
S0, 2x
20 µm
S0, 40x
1 µm
S1Na, 1.5x
30 µm
S1Na, 10x
5 µm
S3Cu (SE-detector)
2 µm
S3Cu (BSE-detector)
2 µm

Fig. 2

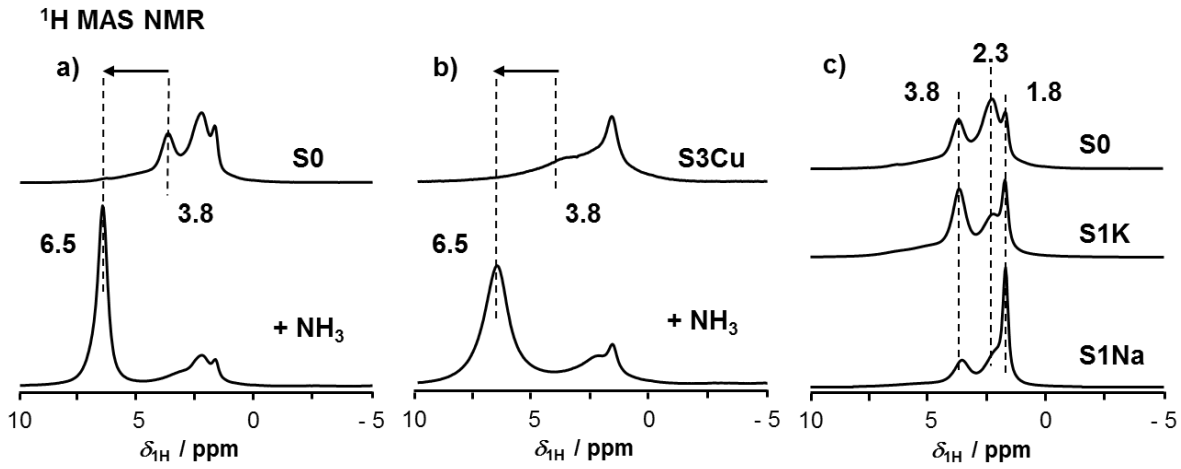
^{1}H MAS NMR
a)
S0
3.8
6.5
+ NH$_3$
10
5
0
- 5
δ_{1H} / ppm
b)
S3Cu
3.8
6.5
+ NH$_3$
10
5
0
- 5
δ_{1H} / ppm
c)
2.3
3.8
1.8
S0
S1K
S1Na
10
5
0
- 5
δ_{1H} / ppm

Fig. 3

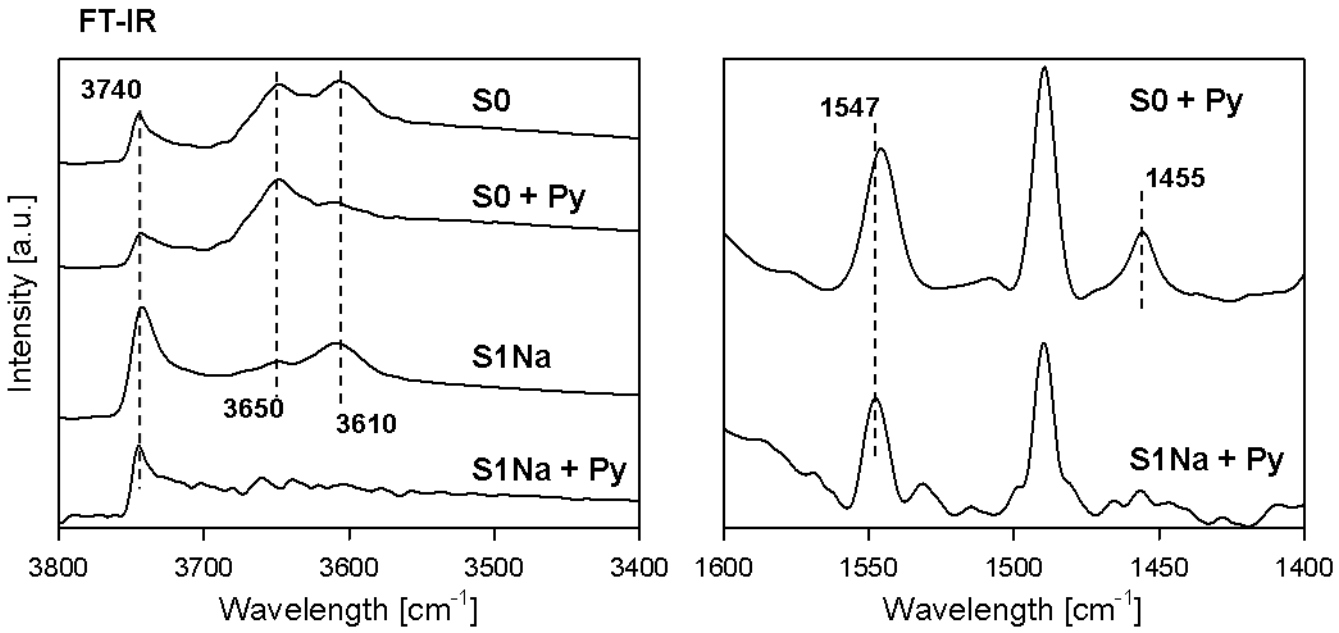
FT-IR
3740
S0
S0 + Py
S1Na
3650
3610
S1Na + Py
Intensity [a.u.]
3800
3700
3600
3500
3400
Wavelength [cm-1]
1547
S0 + Py
1455
S1Na + Py
1600
1550
1500
1450
1400
Wavelength [cm-1]

Fig. 4

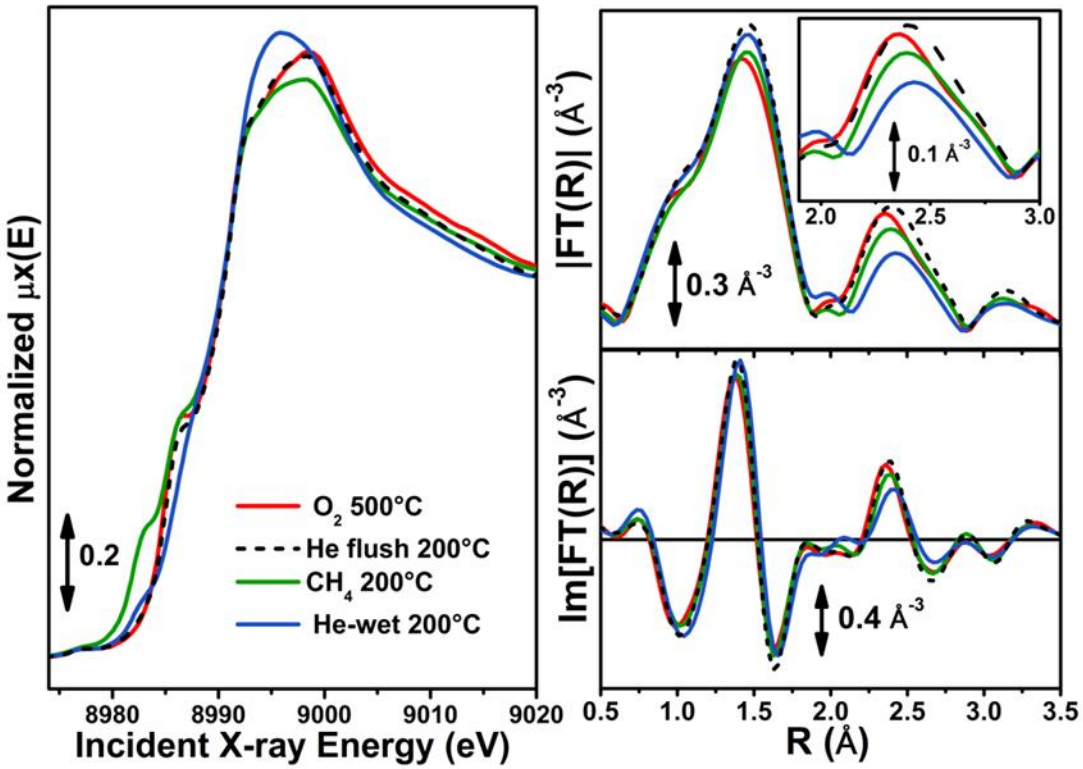
Normalized μx(E)
0.2
O2 500°C
He flush 200°C
CH4 200°C
He-wet 200°C
8980
8990
9000
9010
9020
Incident X-ray Energy (eV)
|FT(R)| (Å-3)
0.3 Å-3
0.1 Å-3
2.0
2.5
3.0
Im[FT(R)] (Å-3)
0.4 Å-3
0.5
1.0
1.5
2.0
2.5
3.0
3.5
R (Å)

Fig. 5

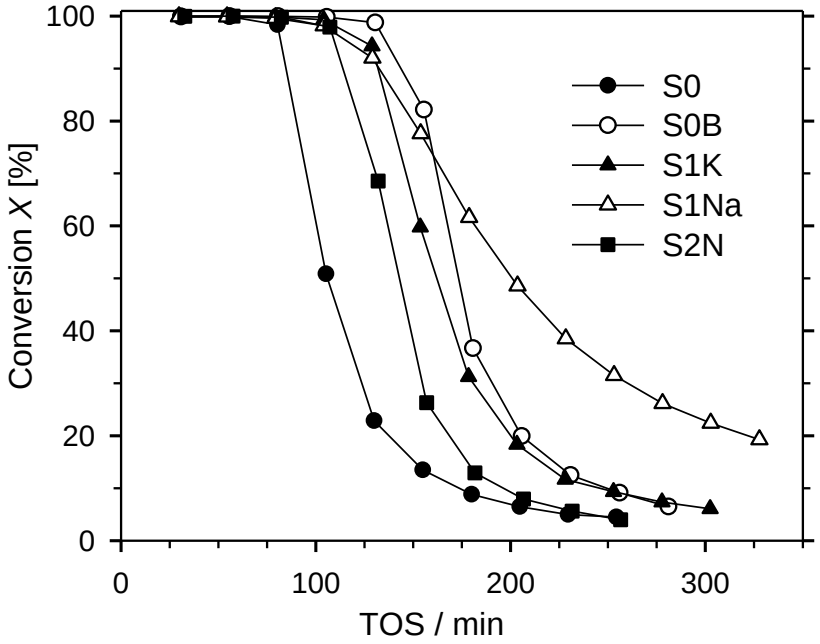
100
80
60
40
20
0
Conversion X [%]
0
100
200
300
TOS / min
S0
S0B
S1K
S1Na
S2N

Fig. 6

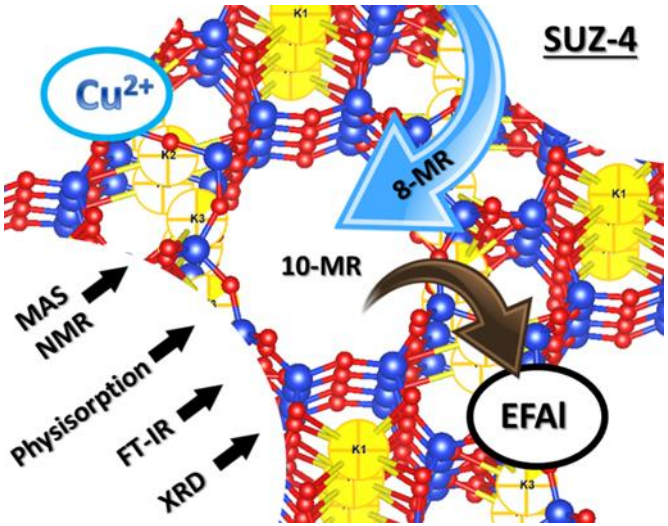
SUZ-4
Cu2+
8-MR
10-MR
EFAl
MAS NMR
Physisorption
FT-IR
XRD
K1
K2
K3

Abstract